


# FOXG1 targets BMP repressors and cell cycle inhibitors in human neural progenitor cells

Nuwan C. Hettige<sup>1,2</sup>, Peter Fleming<sup>2,3</sup>, Amelia Semenak<sup>2,3</sup>, Xin Zhang<sup>2</sup>, Huashan Peng<sup>2</sup>, Marc-Daniel Hagel<sup>4</sup>, Jean-François Théroux<sup>2</sup>, Ying Zhang<sup>2</sup>, Anjie Ni<sup>1,2</sup>, Malvin Jefri<sup>2,3</sup>, Lilit Antonyan<sup>1,2</sup>, Shaima Alsuwaidi<sup>2,3</sup>, Andreas Schuppert<sup>4</sup>, Patrick S. Stumpf<sup>4</sup> and Carl Ernst <sup>1,2,3,5,\*</sup>

<sup>1</sup>Department of Human Genetics, McGill University, Montreal, QC H3A 0C7, Canada

<sup>2</sup>Psychiatric Genetics Group, Montreal, QC H4H 1R3, Canada

<sup>3</sup>Department of Neurology and Neurosurgery, McGill University, Montreal, QC H3A 2B4, Canada

<sup>4</sup>Joint Research Center for Computational Biomedicine, RWTH Aachen University, Aachen 52074, Germany

<sup>5</sup>Montreal Neurological Institute, McGill University, Montréal, QC H3A 2B4, Canada.

\*To whom correspondence should be addressed at: Carl Ernst, Douglas Mental Health University Institute, 6875 Boulevard LaSalle, Montreal, QC H4H 1R3, Canada. Tel: +1 5147616131 ext.: 3382; Fax: +1 5147623023; Email: carl.ernst@mcgill.ca

## Abstract

FOXG1 is a critical transcription factor in human brain where loss-of-function mutations cause a severe neurodevelopmental disorder, while increased FOXG1 expression is frequently observed in glioblastoma. FOXG1 is an inhibitor of cell patterning and an activator of cell proliferation in chordate model organisms but different mechanisms have been proposed as to how this occurs. To identify genomic targets of FOXG1 in human neural progenitor cells (NPCs), we engineered a cleavable reporter construct in endogenous FOXG1 and performed chromatin immunoprecipitation (ChIP) sequencing. We also performed deep RNA sequencing of NPCs from two females with loss-of-function mutations in FOXG1 and their healthy biological mothers. Integrative analyses of RNA and ChIP sequencing data showed that cell cycle regulation and Bone Morphogenic Protein (BMP) repression gene ontology categories were over-represented as FOXG1 targets. Using engineered brain cell lines, we show that FOXG1 specifically activates SMAD7 and represses CDKN1B. Activation of SMAD7 which inhibits BMP signaling may be one way that FOXG1 patterns the forebrain, while repression of cell cycle regulators such as CDKN1B may be one way that FOXG1 expands the NPC pool to ensure proper brain size. Our data reveal novel mechanisms on how FOXG1 may control forebrain patterning and cell proliferation in human brain development.

## Introduction

FOXG1 heterozygous loss-of-function mutations cause FOXG1 syndrome (1) (OMIM 164874), a severe neurological disorder where individuals frequently show absent speech, intractable seizures, motor anomalies, reduced cortical size, agenesis of the corpus callosum and hypoplasia of the basal ganglia (2,3). It is not known why heterozygous loss-of-function mutations in FOXG1 cause such severe neurological defects in the human brain.

*Foxg1* is brain expressed (4) and there is significant support for a role in expanding the neural progenitor cell (NPC) pool, that is, increasing proliferation of NPCs (5). *Foxg1* knock-out (–/–) mice have absent or extremely stunted cerebral cortices (6,7) caused by premature exit from the cell cycle of NPCs during their expansion phase as evidenced by an increased frequency of cells in G1/G0 phase (6–8), a result we confirmed in human NPCs (9). Furthermore, FOXG1 is among the most consistently over-expressed genes in glioblastoma multiforme (10–13), one of the most deadly cancers in humans (14). The level of FOXG1 protein available in the cell, or dosage, appears to be critical in tuning cell proliferation, since too much is associated with cancer and too little causes microcephaly (5). It is not known why *Foxg1* is dosage sensitive but there have been some targeted attempts to investigate this phenomenon with respect to NPC expansion in animal models (15,16).

*Foxg1* is associated with forebrain patterning, meaning it helps influence the identification of cells along the body axes in the forebrain. The body axes are divided along anterior/posterior and dorsal/ventral axes and cell specification is a consequence of a progenitor cell's position in 3D space and susceptibility to the combination of different concentrations of morphogens. Several studies have reported that *Foxg1* may influence cell patterning by inhibiting the BMP family (17) to make cells competent to ventralize (18), but how *Foxg1* might repress Bmp signaling is controversial (19). One study reported that complete loss of *Foxg1* led to ectopic expression of Bmp ligands in embryonic brain, suggesting *Foxg1* may repress Bmp morphogens (8). Another study describes *Foxg1* interaction with *Foxh1* (also known as *Fast2*) (20), which act to block the association and translocation of activating Smads. Smads are signal transduction molecules that relay information from receptors at the cell surface to the nucleus. Yet another describes an association between *Foxo3a* and *Foxg1* which blocked Smad translocation to the nucleus (15). While it is possible that all these mechanisms function additively to inhibit Bmp signaling, each is focused on protein–protein interactions with *Foxg1*, ignoring the presumed critical role of *Foxg1* as a transcriptional regulator.

FOXG1 is a member of the FOX (Forkhead box) superfamily characterized by the amino acid forkhead winged helix domain

that associates with DNA (21,22). The FOX domain is a winged helix of approximately 100 amino acids that binds to the Forkhead DNA binding (FDB) motif. This motif is comprised of nucleotides, TRTTRY (23) (or reverse complement RYAAAYA), where R is a purine (A/G) and Y is a pyrimidine (C/T), which has even been independently confirmed for the specific forkhead amino acid sequence in *Foxg1* (24). To date, there have been three ChIPseq studies in post-mitotic neurons from mice (25–27) and one done in human brain tumor samples (28) to understand where *Foxg1* may bind in the genome, though none in healthy human cells. Here, we perform a FOXG1 ChIPseq experiment in healthy human NPCs and integrate ChIPseq data with RNAseq data from subjects with FOXG1 mutations. We reason that proof of differential expression in FOXG1 syndrome cases and controls combined with clear evidence of binding in FDB motifs of these same genes constitutes reasonable evidence for direct effects of FOXG1. We follow up these data for two genes by genetically tuning FOXG1 levels to demonstrate their direct control by FOXG1.

## Results

### Transcriptomic changes in NPCs with pathogenic FOXG1 mutations

To investigate transcriptomic differences caused by FOXG1 haploinsufficiency, we utilized two FOXG1 syndrome cases and their sex-matched familial controls to assess differential gene expression. Case A has a ~4 MB deletion on chromosome 14 that encompasses FOXG1 (14q12 del), and Case B has a 1 bp frameshift mutation in FOXG1 (c.256dup) (Fig. 1A; Supplementary Material, Table S1). We derived iPSCs from all four lines and differentiated them into NPCs (29,30) which expressed standard NPC markers (Fig. 1B), and with which we have already described in full (9). FOXG1 syndrome cases show decreased FOXG1 protein levels compared to family and sex-matched control NPCs (Fig. 1C). We performed RNAseq using two replicates per sample for a total of eight samples, with over 100 M reads generated per sample.

From 43051 expressed genes, there were 2124 that were significantly differentially expressed at FDR  $q < 0.05$ . We observed 1278 down-regulated and 846 up-regulated genes in FOXG1 syndrome cases compared to controls (Fig. 1D). Pathway and gene ontology (GO) term enrichment analysis of down-regulated genes included 'negative regulation of pathway-restricted SMAD protein phosphorylation' (Supplementary Material, Fig. S1A). Genes involved in SMAD pathway regulation that were differentially expressed include *NOG* (log<sub>2</sub> fold change = -1.40,  $q = 1.94 \times 10^{-7}$ ), *BAMBI* (log<sub>2</sub> fold change = -1.50,  $q = 4.60 \times 10^{-3}$ ), *GDF7* (log<sub>2</sub> fold change = -2.32,  $q = 3.83 \times 10^{-4}$ ), *SMAD6* (log<sub>2</sub> fold change = -0.67,  $q = 2.88 \times 10^{-6}$ ) and *SMAD7* (log<sub>2</sub> fold change = -1.00,  $q = 9.06 \times 10^{-5}$ ). Notably, decreased BMP repression/inhibition potentially causes increased cell differentiation and dorsalization (31), a result consistent with small brain size and loss of ventral markers observed in mouse *Foxg1* knock-out models (18,32). We also observed genes involved in telencephalon regionalization and forebrain cell proliferation including *SIX3* (log<sub>2</sub> fold change = -2.88,  $q = 1.29 \times 10^{-3}$ ), *EMX2* (log<sub>2</sub> fold change = -3.21,  $q = 8.06 \times 10^{-3}$ ), *SHH* (log<sub>2</sub> fold change = -2.20,  $q = 0.01$ ), *EOMES* (log<sub>2</sub> fold change = -2.87,  $q = 0.02$ ), *ARX* (log<sub>2</sub> fold change = -1.74,  $q = 0.02$ ) and *LHX5* (log<sub>2</sub> fold change = -1.61,  $q = 0.02$ ). These changes are consistent with patterning defects observed in *Foxg1* mutation models.

GO analysis of significantly up-regulated genes revealed a strong enrichment for genes associated with 'cilium assembly', 'neurogenesis' and 'brain development' (Supplementary Material,

Fig. S1B). An enrichment for genes involved in cilium assembly included *IFT140* (log<sub>2</sub> fold change = 0.35,  $q = 2.82 \times 10^{-3}$ ), *CEP131* (log<sub>2</sub> fold change = 0.23,  $q = 7.74 \times 10^{-4}$ ), *IFT74* (log<sub>2</sub> fold change = 0.28,  $q = 0.03$ ) and *CEP170* (log<sub>2</sub> fold change = -0.15,  $q = 8.96 \times 10^{-3}$ ). This result is consistent with our recent findings indicating increased frequency of primary cilia in NPCs from FOXG1 syndrome cases (9). Genes related to 'neurogenesis' and 'brain development' (many genes were common to both categories) included *NRXN3* (log<sub>2</sub> fold change = 1.37,  $q = 2.87 \times 10^{-2}$ ), *NRN1* (log<sub>2</sub> fold change = 1.36,  $q = 5.04 \times 10^{-3}$ ), *SLIT1* (log<sub>2</sub> fold change = 1.20,  $q = 6.79 \times 10^{-23}$ ), *CEND1* (log<sub>2</sub> fold change = 1.54,  $q = 1.86 \times 10^{-10}$ ), *CDK5RAP2* (log<sub>2</sub> fold change = 0.22,  $q = 1.96 \times 10^{-3}$ ) and *TUBB2B* (log<sub>2</sub> fold change = 0.21,  $q = 3.19 \times 10^{-5}$ ). Increased expression of genes in these categories is consistent with premature neuronal differentiation and early exit from the cell cycle.

To support our RNAseq findings, we confirmed expression differences at the protein level by performing immunocytochemistry experiments for selected target genes in one category of particular interest, 'negative regulation of BMP signaling pathway'. We observed decreases in cases compared to controls in *BAMBI* (Fig. 1E and F) and *SMAD6* in NPCs (Fig. 1G and H).

### FOXG1 ChIP demonstrates enrichment for genome-wide binding at FDB consensus sites in human NPCs

Our RNAseq results provide important evidence for the downstream molecular consequences of FOXG1 haploinsufficiency; however, it is difficult to determine if these are direct or indirect effects on gene expression. To investigate whether gene expression changes may be due directly to FOXG1 binding and transcriptional control in cis, we performed ChIP sequencing in healthy control NPCs. We first tested the validity of our FOXG1 antibody for use in Western blot and immunoprecipitation (IP). We transfected HEK293 cells with a FOXG1-FLAG construct and performed IP for FLAG with a Western Blot for FOXG1 to confirm the presence of a band at the expected size (58 kDa) for FOXG1 (Fig. 2A). This result, in addition to the observed depletion of FOXG1 in our NPCs with FOXG1 mutations used in the RNAseq (Fig. 1C), indicates that this antibody reliably detects human FOXG1. To confirm the validity of this antibody for IP, we transfected HEK cells with our FOXG1-FLAG construct and performed IP for FOXG1 and western blot for FLAG. Here, we observed a clear band for FLAG in our FOXG1 IP condition (Fig. 2B).

We previously noticed FOXG1 protein level variation as a function of developmental state (9). Specifically, FOXG1 levels are maximal in the NPC state and if NPCs are even slightly differentiated or not yet fully induced, FOXG1 levels are drastically lower (9). We reasoned that using our FOXG1-reporter line where we tagged tdTomato-2A into endogenous FOXG1 (Fig. 2C) would allow us to visually ensure maximal FOXG1 protein levels at the exact developmental time state when we performed ChIPseq. The 2A system leads to the translation of two separate peptides (tdTomato and FOXG1) from the same RNA strand (33), with no change to endogenous FOXG1 protein function (Fig. 2D). We made this cell line using our simultaneous reprogramming and CRISPR/Cas9 protocol for homology directed repair (HDR) (34). Sequencing was performed on a pooled sample of five independent replicates of ChIP (separate wells, separate IPs, but pooled sequencing). A corresponding input from the tdTomato-FOXG1 line was used with matching run type, read length and replicate structure as the FOXG1-IP samples for normalization.

Following ENCODE standards (35), we found that FOXG1 samples yielded genomic distributions that were highly enriched for

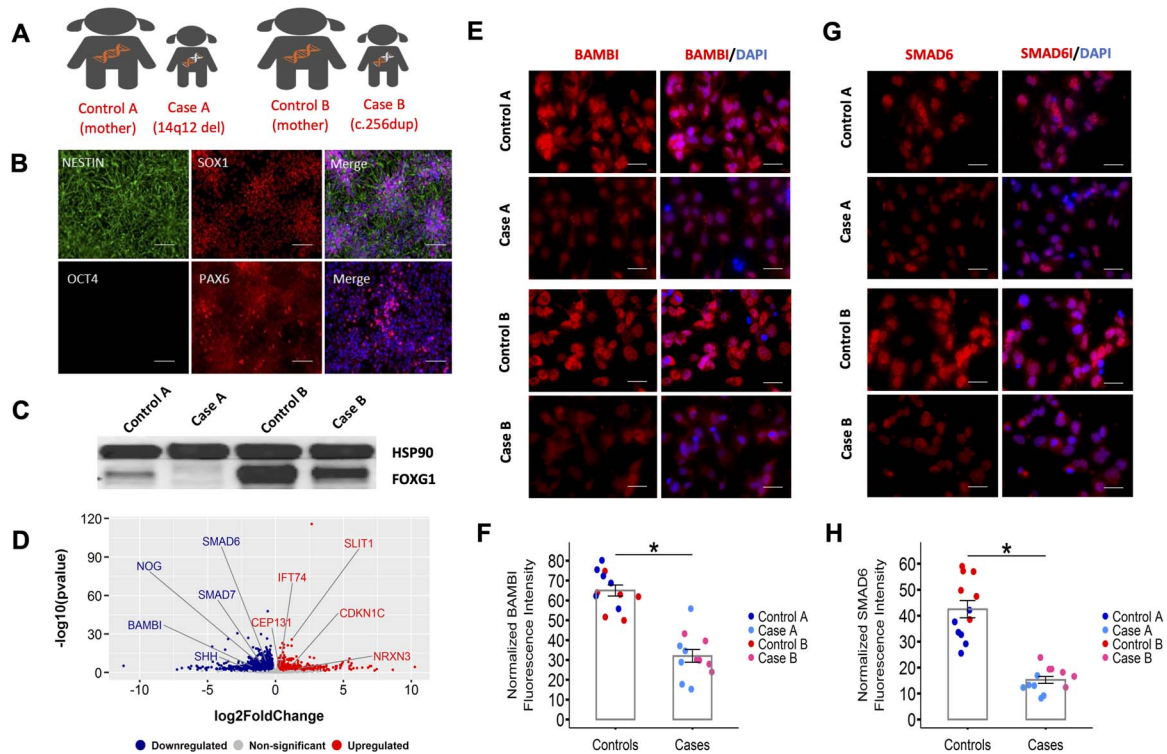


**Figure 1.** Genes regulating BMP signaling, development and cilium assembly are differentially expressed in neural progenitor cells (NPCs) with pathogenic FOXG1 mutations. **(A)** Illustrative diagram of FOXG1 Syndrome cases, their genetic mutations and matched controls. **(B)** Representative immunofluorescence images of NPCs stained for standard forebrain neural progenitor markers and the pluripotency marker, OCT4. The scale bar represents 50  $\mu\text{m}$ . **(C)** Western blot detecting endogenous FOXG1 in human NPCs demonstrating loss of FOXG1 in Case A and B NPCs compared to sex-matched family controls. **(D)** Volcano plot of differentially expressed genes that are up-regulated and down-regulated according to the nominal P-value. **(E)** Representative immunofluorescence of BAMBI with DAPI stain in forebrain NPCs. The scale bar represents 25  $\mu\text{m}$ . **(F)** Quantification of BAMBI-positive NPCs in cases versus matched controls ( $n=2$  controls and 2 cases; 6 images from 6 independent replicates quantified per line for a total of 24 experiments). Error bars denote SEM. Significance stars are based on student's t-test (\*\* $P < 0.005$ ). **(G)** Representative immunofluorescence of SMAD6 with DAPI stain in forebrain NPCs. The scale bar represents 25  $\mu\text{m}$ . **(H)** Quantification of SMAD6-positive NPCs in all cases versus matched controls ( $n=2$  controls and 2 cases; 6 images from 6 independent replicates quantified per line for a total of 24 experiments).

peaks at promoter regions [ $<1$  kb from transcription start sites (TSS)], introns and distal intergenic regions (Fig. 2E). Approximately 17% of genomic loci bound by FOXG1 were within 1 kb of TSS (Supplementary Material, Fig. S2A) which is highly unlikely to be due to chance given that these represent  $<0.1\%$  of the genome (36,37). In total, we identified 124001 peaks at a Benjamini-Hochberg  $q$ -value  $< 0.05$  throughout the genome predicted to be genomic loci bound by FOXG1 (Supplementary Material, Fig. S2B). To identify peaks overlapping a FOXG1 FDB motif (TRTTTRY or reverse complement), we selected those peaks within or near an FDB motif up to a maximum distance of 100 bp upstream and downstream of peak range coordinates (38). There were 41935 peaks that contained an FDB motif ( $\sim 33\%$ ), and we annotated these according to their nearest gene and several of these peaks contained multiple FDB motifs (Fig. 2F). In the supplemental information, we provide an analysis of select gene categories with promoter-bound FOXG1 to FDB motifs (Figures S3–S7). There are many highly significant peaks that do not contain FDB motifs that may indicate FOXG1 binding at non-canonical regions. These were not analyzed in the current work.

### Significantly differentially expressed genes enriched for FOXG1 DNA binding motifs are associated with cell proliferation, BMP signaling and neuronal differentiation

To assess whether genes with ChIP peaks with FDB motifs (in the gene or within 2 kb 5' and 3' of TSS/TTS) were also

significantly differentially expressed in FOXG1 syndrome cases compared to controls, we integrated FOXG1 ChIPseq and our case/control RNAseq analysis. We selected genes with ChIPseq peaks that overlapped with an FDB motif that were also present in our RNAseq at  $q < 0.05$ . We integrated the 2124 significant RNAseq genes and the 14247 unique genes annotated to 41935 ChIPseq peaks with an FDB motif to obtain a final list of 4297 peaks with 1231 unique genes that overlapped ChIP and RNAseq datasets (Fig. 3A; Supplementary Material, Fig. S8). Gene set enrichment analysis of the 1231 gene lists had multiple GO terms associated with 'cell cycle' and 'cell proliferation' (Fig. 3B), as well as 'negative regulation of SMAD protein phosphorylation'. Looking at cell proliferation categories (ChIP peaks are shown in Figure 3C, RNAseq values shown here in the text as fold change difference from control), we observe CDKN1B (log<sub>2</sub> fold change = 0.24;  $q = 2.20 \times 10^{-3}$ ), CDKN1C (log<sub>2</sub> fold change = 1.03;  $q = 6.45 \times 10^{-3}$ ) and CCNDBP1 (log<sub>2</sub> fold change = 0.17;  $q = 1.31 \times 10^{-2}$ ) as being up-regulated in FOXG1 syndrome cases, while CDC25A (log<sub>2</sub> fold change = -0.13;  $q = 0.03$ ), MASTL (log<sub>2</sub> fold change = -0.32;  $q = 1.05 \times 10^{-3}$ ) and CCND3 (log<sub>2</sub> fold change = -0.29;  $q = 0.03$ ) are down-regulated in FOXG1 syndrome cases. CDC25A, MASTL (also known as Greatwall Kinase (39)) and CCND3 are drivers of cell cycle progression (40–42), and are thus increased by FOXG1 in healthy conditions. CDKN1B, CDKN1C and CCNDBP1 (43) are inhibitors of the cell cycle and are thus normally repressed by FOXG1 in healthy conditions. All ChIPseq peaks are in promoters and are highly significant: CDKN1B ( $-\log_{10} q = 22.51$ ), CDKN1C



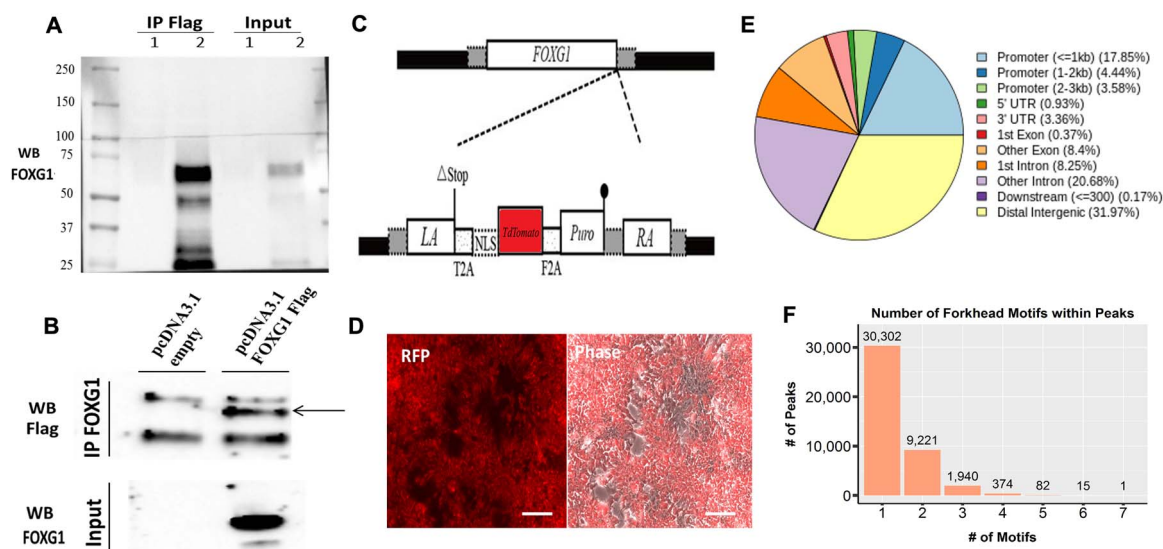


**Figure 2.** Immunoprecipitation (IP) and ChIPseq of endogenous FOXG1-tdTomato in human neural progenitor cells (NPCs) identifies peaks at forkhead binding motifs across genomic features. **(A)** Detection of transfected FOXG1-FLAG vector in HEK293 cells which do not endogenously express FOXG1. IP for FLAG and western blot for FOXG1 confirms antibody detection of FOXG1 at about ~62 kDa (1 = pcDNA3.1 empty vector; 2 = pcDNA3.1 FOXG1-FLAG). **(B)** IP for FOXG1 and western blot for FLAG confirms antibody detection of FOXG1 and ability to pull down FOXG1 using ab196868 antibody (1 = pcDNA3.1 empty vector; 2 = pcDNA3.1 FOXG1 FLAG). **(C)** Schematic diagram of FOXG1-reporter construct integrated into the FOXG1 locus in a control NPC line with CRISPR HDR. A tdTomato (tandem dimer Tomato) reporter was integrated into the 3' end of FOXG1 for visualization of FOXG1 in live cells. The components of the construct are as follows: RA = right arm; LA = left arm; NLS = nuclear localization signal; T2A and F2A = two types of 2A signaling to enable translational gapping between two proteins; Stop = stop codon; Puro = puromycin resistance gene. **(D)** Representative images of FOXG1-tdTomato visualized in FOXG1 reporter NPCs. tdTomato expression is visualized using RFP fluorescent channel settings and under phase-contrast microscopy conditions (10 $\times$  magnification) in FOXG1 reporter NPCs. **(E)** Pie plot visualization of genomic features annotated to called ChIP peaks. **(F)** Bar plot quantifying the number of peaks with one or more FOXG1 DNA-binding motifs. About 28% of peaks had two or more FBD motifs.

( $-\log_{10} q = 78.08$ ), CCNDBP1 ( $-\log_{10} q = 80.88$ ), CDC25A ( $-\log_{10} q = 9.44$ ), MASTL ( $-\log_{10} q = 37.86$ ) and CCND3 ( $-\log_{10} q = 8.77$ ). We conclude that when FOXG1 dosage is reduced, cell cycle progression is inhibited both by loss of activation of cell cycle drivers and loss of repression of cell cycle inhibitors. FOXG1 appears to directly bind these specific genes in cis, possibly suggesting a direct effect on their expression.

We next segregated overlapping ChIPseq and RNAseq hits according to whether gene expression was up-regulated or down-regulated (Fig. 4A). GO analysis of down-regulated genes with peaks overlapping an FDB motif (830 genes) revealed multiple terms associated with TGF- $\beta$  pathway regulation including, 'negative regulation of BMP signaling pathway' and 'negative regulation of pathway-restricted SMAD protein phosphorylation' (Supplementary Material, Fig. S8A). Within the promoter region of SMAD6, we observe one of the most significant peaks in our dataset ( $-\log_{10} q = 216.71$ ) which contained two FDB motifs in a single peak (Fig. 4B). SMAD7 also has a highly significant peak ( $-\log_{10} q = 49.61$ ). We see extremely significant peaks and RNAseq  $q$ -values for the SMAD inhibitors, [SMAD6 (RNAseq: log<sub>2</sub> fold change =  $-0.665$ ;  $q = 2.88 \times 10^{-6}$ ) and SMAD7 (log<sub>2</sub> fold change =  $-1.00$ ;  $q = 9.06 \times 10^{-5}$ )], suggesting that SMAD6 and SMAD7 are bound by FOXG1 to activate expression. Increasing the expression of these two known inhibitors of SMAD signaling is a novel explanation as to how FOXG1 may block TGF- $\beta$ /BMP signaling. Other inhibitors of BMP expression were also detected, meaning FOXG1 may directly target and activate several proteins that repress TGF- $\beta$ /BMP signaling. BAMBI (ChIPseq log<sub>10</sub>  $q = 6.59$ ) and GDF7 (ChIPseq log<sub>10</sub>  $q = 11.04$ ) both have a single FOXG1 peak in their promoter regions and are also significantly down-regulated in FOXG1 syndrome cases.

GO analysis of genes that were up-regulated with peaks overlapping an FDB motif (401 genes) (Fig. 4C) revealed multiple

terms related to axon guidance, including 'retinal ganglion cell axon guidance', 'negative regulation of axon extension involved in axon guidance', 'regulation of axon extension involved in axon guidance' and 'axon guidance' as top-ranked GO terms (Supplementary Material, Fig. S8B). In addition, there were multiple terms related to neuron differentiation, including 'neuron differentiation', 'neuron development', 'generation of neurons' and 'neurogenesis'.

Looking at neuron differentiation genes (Fig. 4D), NRN1 has five peaks, including one right in the promoter ( $-\log_{10} q = 15.50$ ), and loss of FOXG1 leads to NRN1 up-regulation (log<sub>2</sub> fold change =  $1.359$ ;  $q = 5.04 \times 10^{-3}$ ) suggesting that FOXG1 may bind NRN1 and repress its expression (44). Another gene of interest implicated in neurodevelopment and disease (45), NRXN3, has one peak ( $-\log_{10} q = 13.05$ ) and is significantly up-regulated in patient NPCs (log<sub>2</sub> fold change =  $1.372$ ;  $q = 0.029$ ). These data may be consistent with premature differentiation of NPCs due to depleted FOXG1 expression.

Loss of FOXG1 may lead to an up-regulation of genes involved in axon guidance and neuronal differentiation leading to what may be premature neuronal differentiation of NPCs (Fig. 4D). In particular, repellent axon guidance genes, SEMA3D and SLIT1 have one peak at their promoter region (SEMA3D:  $-\log_{10} q = 2.65$ ; SLIT1:  $-\log_{10} q = 15.75$ ) and are both significantly up-regulated in patient NPCs (SEMA3D: log<sub>2</sub> fold change =  $0.834$ ;  $q = 1.43 \times 10^{-3}$ ; and SLIT1: log<sub>2</sub> fold change =  $1.196$ ;  $q = 6.79 \times 10^{-23}$ ). These data show increased expression of certain axon guidance molecules, many of which are repressive. This may be consistent with the loss of corpus callosum fibers, though these data need to be pursued further given expression is observed in unpolarized NPCs.

We also assessed whether FOXG1 binding sites and gene targets identified here are concordant across other studies that have investigated FOXG1 binding and gene regulation. Specifically, we

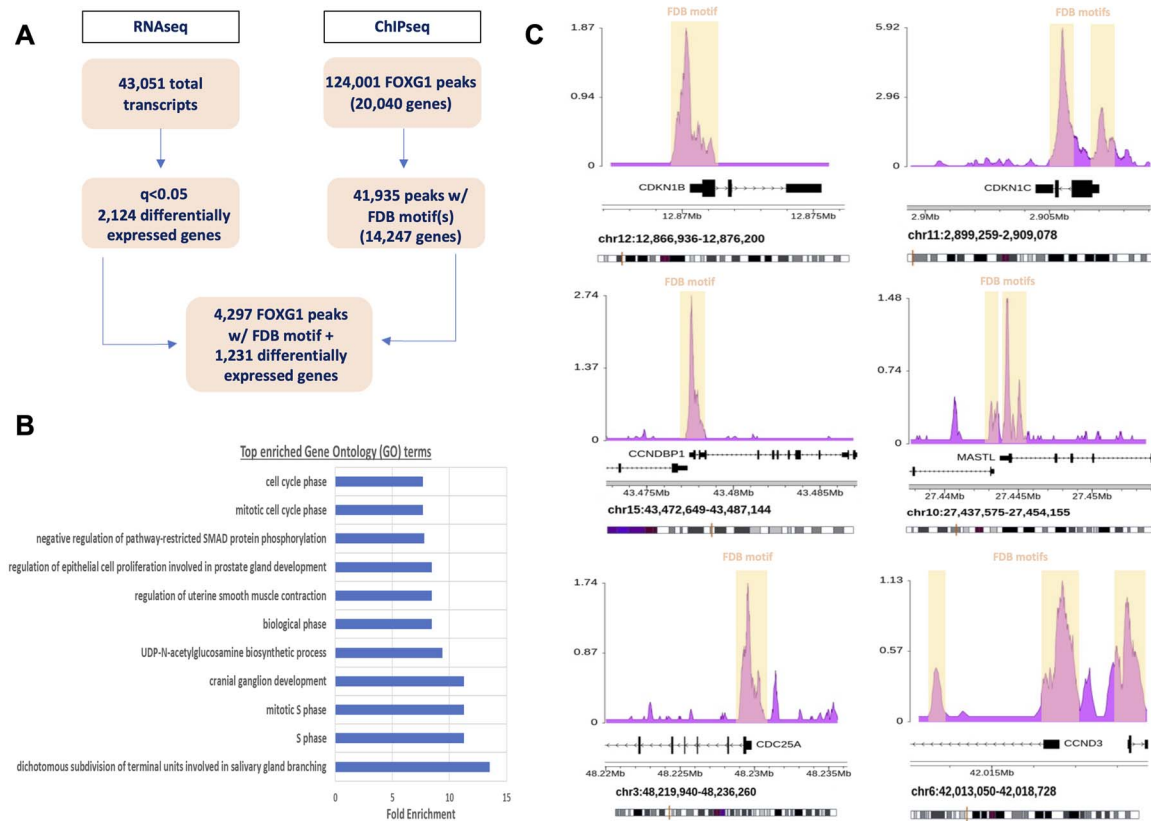


**Figure 3.** Integrated analysis of RNAseq and ChIPseq reveal enrichment for regulators of the cell cycle. **(A)** Flow chart demonstrating the number of genes differentially expressed in the RNAseq and genes annotated to peaks in the ChIPseq analyses that overlap. **(B)** Top enriched Gene Ontology terms ranked according to fold enrichment. **(C)** Visualization of ChIPseq peaks with FOXG1 DNA-binding (FDB) motifs highlighted for genes also identified in the RNAseq analysis with significant roles in cell cycle and cell proliferation (CDKN1B, CDKN1C, CCNDBP1, MASTL, CDC25A and CCND3). Y-axis represents normalized read depth, where the height of peaks reflects read depth above normalized baseline.

compared our findings to those of Kumamoto *et al.* (2013), Dali *et al.* (2018) and Cargnin *et al.* (2018) (Supplemental information).

### Direct evidence that FOXG1 levels drive expression of CDKN1B and SMAD7

The ChIP/RNAseq data suggest that FOXG1 binds to and drives expression of critical genes in cell proliferation and patterning. We chose to specifically investigate this model on two specific genes relevant to BMP repressors and cell cycle inhibitors. We first tested both BAMBI and SMAD6 antibodies since these were available from our initial ICC experiments, but we were unable to confirm western blot band specificity. We opted next to test SMAD7 and CDKN1B and assessed protein levels in both cases and controls to ensure protein levels were consistent with RNAseq. We observed decreases in SMAD7 and increases of CDKN1B in FOXG1 syndrome case NPCs compared to control NPCs (Fig. 5A), suggesting that FOXG1 normally activates SMAD7 and represses CDKN1B in healthy NPCs. We also transfected FOXG1 into NPCs to directly determine if the presence of FOXG1 affects protein levels (Fig. 5B). We found FOXG1 transfection increased SMAD7 levels and decreased CDKN1B levels. We also created an inducible FOXG1 over-expression (OE) line in Case B (see Supplementary Material, Fig. S9 for vector cloning design). Using CRISPR-guided homology direct repair, we created a dox-inducible FOXG1-FLAG-2A-RFP transgene in the human Citrate Lyase Beta-Like (CLYBL) locus, which we call FOXG1-OE. After neural induction (Fig. 5C) and application of doxycycline to NPC cultures, we found increases in SMAD7 and decreases in CDKN1B, supporting a direct role for

FOXG1 on these genes using stably inserted, inducible FOXG1 (Fig. 5D).

### Discussion

Most mechanistic studies of *Foxg1* have been done in homozygous mutant animals despite the critical role of FOXG1 haploinsufficiency in human cortical expansion (46). It was in this context that we undertook the current study in proliferating human forebrain NPCs. We started with no a priori hypothesis of what FOXG1 may do, but rather took an integrational approach to investigate the effects of FOXG1 DNA binding on gene expression patterns. We found that FOXG1 has robust effects on cell cycle inhibitors and BMP repressors.

*Foxg1* was initially reported to be a repressor (47–49) but this is likely just one of its functions. Indeed, no forkhead protein is defined as solely ‘repressive’ or ‘activational’ on transcription (50,51), so it would be peculiar for FOXG1 to have a uniquely repressive function. Transcription factors such as FOXG1 can have varying effects on transcription usually as a function of binding partners, whereas FOXG1 likely functions to guide repressive or activating partners to the genome. FOXG1 may be repressive, for example by interacting with KDM5B (52), binding to the genome and leading to the removal of H3K4 methylation, an activational mark. One can imagine different repressive (53) and activating proteins interacting with FOXG1 at different developmental time-points. In the current study, we clearly detect both increased and decreased expression patterns in FOXG1 reduced dosage NPCs

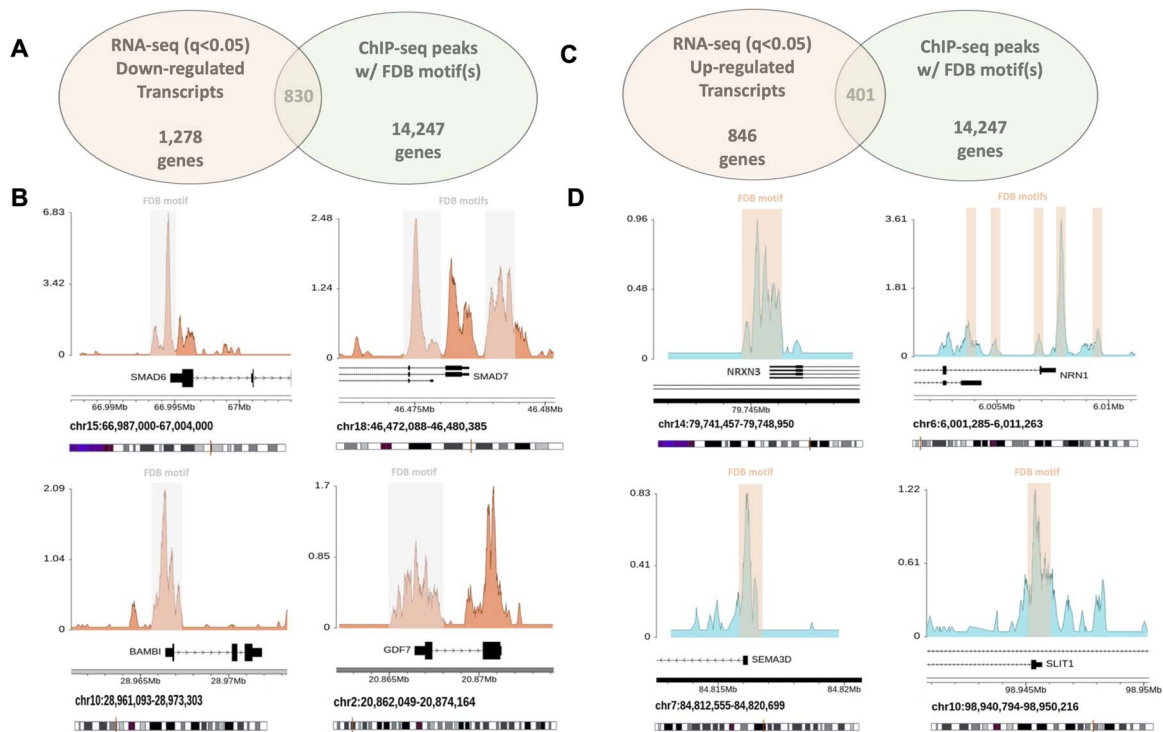


**Figure 4.** Loss of FOXG1 is associated with decreased expression of BMP repressor genes and increased expression of neurogenic and axon guidance genes. **(A)** Venn diagram highlighting the number of genes identified from RNAseq at  $q < 0.05$  that are down-regulated and ChIPseq with peaks at FOXG1 DNA-binding (FDB) motifs. **(B)** Visualization of ChIPseq peaks with FDB motifs highlighted for genes identified in the integrated analysis with significant roles in SMAD and BMP signaling pathways (SMAD6, SMAD7, BAMBI and GDF7). **(C)** Venn diagram highlighting the number of genes identified from RNAseq at  $q < 0.05$  that are up-regulated and ChIPseq with peaks at FOXG1 DNA-binding (FDB) motifs. **(D)** Visualization of ChIPseq peaks with FOXG1 DNA-binding (FDB) motifs highlighted for genes identified in the integrated analysis with significant roles in SMAD and BMP signaling pathways (NRXN3, NRN1, SEMA3D and SLIT1).

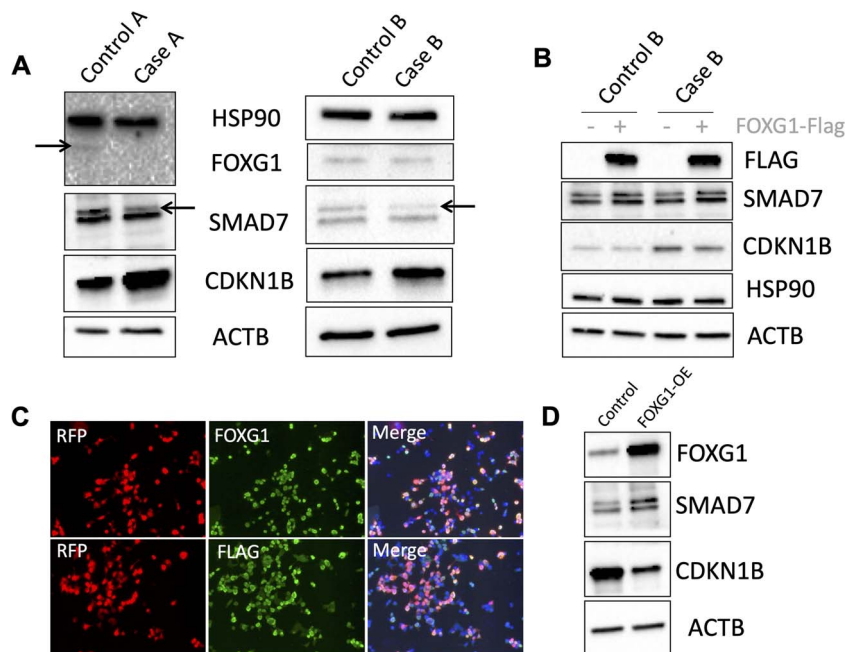


**Figure 5.** Molecular tuning of SMAD7 and CDKN1B levels in human neural progenitor cells (NPCs) by FOXG1. **(A)** Western blot experiments from two cases and two controls showing reduction of SMAD7 and increase of CDKN1B in NPCs from FOXG1 syndrome cases. **(B)** Transient transfection of FOXG1 in NPCs from one case and one control increases SMAD7 and decreases CDKN1B in both FOXG1 mutant and wild-type cells. **(C)** Example of cells that endogenously over-express FOXG1-FLAG-RFP from the CLYBL safe harbor locus. **(D)** FOXG1 Over-Expression (OE) in Case B with doxycycline application at the NPC stage increases SMAD7 and decreases CDKN1B.

and we suggest that at least some of these may be direct effects of FOXG1 binding to these particular genes. To date, no activator-binding protein has been identified with FOXG1 but our work suggests that there is one and that it should be detectable in human NPCs. We also cannot rule out other regulatory functions of FOXG1 such as RNA processing as has been reported for a forkhead homolog in yeast (54).

Loss-of-function mutations in FOXG1 may lead to the large number of molecular changes observed here and could underlie the structural brain deficits that are characteristic of FOXG1 syndrome (1). Control of cell cycle is critical for determining the size of the NPC pool that eventually populates the forebrain and determine its size. One type of powerful cell cycle regulator is the cyclin-dependent kinase (CDK) inhibitor proteins, *CDKN1A* (55), *CDKN1B* (56) and *CDKN1C* (57), whose expression can promote cell cycle arrest, as they have the ability to block CDK-cyclin complexes (58), where combinations of cyclins and CDK heterodimers are essential for progression through the cell cycle (59). Here, we see significant peaks at promoters and differential gene expression of *CDKN1B* and *CDKN1C* (60), possibly suggesting that FOXG1 helps regulate the total number of cell divisions for NPC expansion and brain size through these regulators. *CDKN1B* is already a known target of other FOX proteins (61), so our work may suggest that FOXG1 binds to common forkhead binding motifs within cell cycle repressors to decrease their expression and drive proliferation. This mechanism could underlie our previous findings where we showed that FOXG1 dose-dependently affects cell cycle dynamics and neuronal differentiation (9).

There were a significant number of FOXG1 target genes known to be implicated in primary microcephaly. Loss-of-function mutations in *CDK5RAP2* (62), *ASPM* (63), *STIL* (64), *CEP152* (65) and *CENPJ* (66) all-cause primary microcephaly and so FOXG1 may normally bind to these genes and increase their expression in NPCs. This suggests that FOXG1 may have evolved very diverse ways of increasing NPC proliferation not only directly influencing the cell cycle but also by regulating genes implicated in centrosomal biology (67). The mitotic spindle is formed from microtubules emanating from centrioles, and these govern chromosomal segregation at mitosis. The microcephaly genes described here influence centriole replication/assembly/stability/binding (68), which is required for both mitosis and primary cilia formation. FOXG1 decreased dosage might increase cilia formation and decrease cell division by regulating important genes in centrosome control.

Many individuals with FOXG1 syndrome show agenesis or impaired development of the corpus callosum. Multiple processes are involved in callosal development and the genetic causes of agenesis are heterogeneous (69,70), including impairment of axon guidance (70). We observed genes involved in axon guidance as targets of FOXG1 binding and regulation, including *SLIT1*, *NRP1* and multiple semaphorins, all of which are up-regulated in FOXG1-depleted NPCs. Axonal guidance cues are categorized as 'attractive' or 'repulsive', with *SLIT1* and *NRP1* and most semaphorins categorized as repulsive (71–73). Our results suggest a high frequency of axon guidance cues in the repulsive category may be under direct control of FOXG1. A previous study in mouse observed *Foxg1* binding and repression of repellent axon guidance cues, *Robo1*, *Slit3* and *Reelin* through the formation of a *Foxg1*-Rp58 complex (26). The loss of axon guidance repression in that mouse study led to callosal axon projections stalled at the midline. Our data provide support for this model but with a wider range of repulsive cues that may fail to be expressed in humans at the proper time and place.

*Foxg1* knock-out models show patterning defects (18,32) that may occur via Bmp inhibition. Here, we have shown that FOXG1

binds to and is an activator of *SMAD6*, *SMAD7* and *BAMBI* expression, amongst others, all of which are repressors of BMP pathways. Lack of repression of BMPs could lead to early differentiation of FOXG1-depleted tissues or patterning defects (74–77).

The dose of FOXG1 in a cell may be a powerful amplifier of even small signaling cues since FOXG1 can potentially drive so many different genes in diverse pathways that converge on the common output. This positive feedback, where FOXG1 drives pathways that in turn amplify other related pathways, may be one mechanism for cells to regulate cell state. The layer upon layer of signaling cascades which can drive different processes are all shifted toward the same goal when a powerful regulator such as FOXG1 is present at high enough levels in a cell. This would also require extensive negative regulation since FOXG1 presence is likely at or near the top of pathway signaling hierarchies.

This work proposes that FOXG1 amplifies cell proliferation signals in part through the activation of BMP repressors and repression of cell cycle inhibitors. Identification of FOXG1 binding partners by developmental state, FOXG1 stability at RNA and protein levels, and confirmation of more FOXG1 targets will be critical to better understand the role of this remarkable protein in brain cells.

## Materials and Methods

### Subjects and cell lines

The FOXG1-reporter line was generated by reprogramming somatic cells into iPSC colonies while simultaneously inserting a tdTomato tag at the end of endogenous FOXG1. Case A is a FOXG1 syndrome patient with a 14q12 heterozygous deletion including FOXG1, whereas Control A is her healthy, biological mother. Somatic cells from both individuals were obtained at the Douglas Hospital Research Institute (Montreal, Canada). Case B and Control B fibroblasts were acquired from the Coriell Institute (GM27244 and GM27246, respectively). Case B has a heterozygous duplication in FOXG1 c.256dup (p.Gln86Profs\*35) causing a frameshift mutation. Further details of all cell lines can be found in Hettige et al. (9) and [Supplementary Material, Table S1](#).

### Somatic cell reprogramming

The reprogramming of iPSCs and induction into NPCs followed previously described protocols generated in our lab (34). Fibroblasts and renal epithelial cells were reprogrammed using episomal reprogramming vectors containing Oct4, Sox2, Myc3/4, Klf4 and ShRNA P53 (ALSTEM) and a Neon Transfection System (Invitrogen, Burlington). A total of  $3.0 \times 10^5$  cells were electroporated and reprogrammed with 3  $\mu\text{g}$  of episomal vectors per reaction. Electroporation parameters for fibroblasts were: 1650 V, 10 ms, 3 pulses and 1400 V, 30 ms width, 1 pulse for RE cells. Following transfection, cells were plated on tissue culture plates coated with Matrigel (Corning) in 10% fetal bovine serum (FBS) DMEM. The following day, the medium was exchanged for fresh 10% FBS DMEM supplemented with 2  $\mu\text{g}/\text{ml}$  puromycin, where applicable (Sigma-Aldrich). Puromycin selection was applied for 48 h, after which the medium was exchanged with fresh TesR-E7 medium (Stem Cell Technologies). During the reprogramming process, TesR-E7 medium was changed every day. After > 21 days, iPSC colonies began to appear and could be seen forming from a single cell. Once colonies formed a distinct border (~500–1000  $\mu\text{m}$  in diameter), cells were detached using ReLeSR medium (Stem Cell Technologies) and plated in mTesR1 medium (Stem Cell Technologies) supplemented with ROCK inhibitor y-27632 (Sigma-Aldrich) at a final concentration of 10  $\mu\text{M}$ .



## Quality control for iPSCs

All iPSCs were rigorously assessed for contamination, pluripotency and genomic integrity using several assays. All cells were tested for mycoplasma contamination (EZ-PCR Mycoplasma Test Kit [Biological Industries]). Pluripotency was assessed by immunostaining with surface and nuclear pluripotency markers and spontaneous 7-day embryoid body differentiation confirmed the capacity to form the three germ layers, as described in further detail in Hettige *et al.* (9).

## Differentiation of iPSCs to forebrain NPCs

Neural induction of iPSCs into forebrain NPCs was done as follows: one day after passaging pure iPSC colonies at low density, Neural Induction Media 1 consisted of DMEM/F12 media supplemented with N2 (Invitrogen), B27 (Invitrogen), BSA (Gibco), SB431542 (Stem Cell Technologies), Noggin (GenScript) and Laminin (Sigma-Aldrich) was added. After 7 days of neural induction media 1, cells were switched to neural induction media 2 consisting of DMEM/F12 media supplemented with N2 (Invitrogen) B27 (Invitrogen), BSA (Gibco), NEAA (Gibco) and Laminin (Sigma-Aldrich). After 12 days, cells were dissociated with Gentle Dissociation Reagent (Stem Cell Technologies) and suspended for 2–3 days for NPC purification on non-adherent plates. Lastly, NPC aggregates were plated on Matrigel-coated plates in STEMdiff™ Neural Progenitor Medium (Stem Cell Technologies) with media exchanged every 3 days. Cells were assessed for NPC morphology and stained for the presence of forebrain NPC markers (NESTIN, SOX1 and PAX6) and the absence of pluripotency markers (OCT4).

## RNA extraction and sequencing

Control and Case NPCs were plated at equal density in three wells of a 6-well plate. Our sample was two cases and two controls sequenced in replicate, where replicates are the same cells grown in different wells but undergoing independent RNA extraction, library preparation and sequencing. Cells were lysed and RNA was extracted using the Presto RNA Extraction Kit (Geneaid). RNA samples with RIN values > 9.0 were submitted to Genome Quebec for library preparation (NEB mRNA stranded Library preparation) and RNA sequencing. Eight libraries were run per lane of an Illumina NovaSeq 6000 S4 flow cell (150 bp paired-end reads) with > 100 million reads per library. For bioinformatic processing, we used FASTX-Toolkit, TopHat, Bowtie2 and Cufflinks2 (78,79) with default parameters to preprocess, align and assemble reads into transcripts, estimate abundance and test differential expression.

## Chromatin immunoprecipitation

We grew FOXG1-reporter NPCs to ~80–90% confluence at the time of fixation and lysing. Cells were then crosslinked by adding 1 ml of cross-linking buffer into each 10-mm dish of 10 ml of NPC maintenance media. Dishes were then kept on a shaker at room temperature for 15 min. 1 ml of 1.25 M glycine was then added to each dish which were then left on a shaker at room temperature for 5 min. Media was aspirated and thoroughly washed twice with cold PBS. After aspirating PBS and ensuring plates were dry, 500  $\mu$ l of cold PBS was added to each plate and scraped using a cell scraper to collect cells in an Eppendorf tube. Cells were centrifuged at 4°C for 5 min at 2000 RPM, with the supernatant discarded. Pellets were then resuspended in 1 ml of NPC-I buffer and centrifuged at 4°C for 5 min at 2000 RPM. The supernatant was discarded and pellets were resuspended in 1 ml of NPC-II buffer. After centrifugation at 4°C for 5 min at 2000 RPM, the supernatant was discarded and pellets were resuspended in 1 ml of shearing buffer supplemented with SIGMAFAST

Protease Inhibitor Tablets (Millipore-Sigma). Cell lysates were then transferred to sonication tubes for sonication (COVARIS). After sonication, samples were centrifuged at 13000 RPM for 10 min at 4°C. The supernatant was kept and transferred to new Eppendorf tubes. The protein concentration of the supernatant was then quantified using a Pierce BCA Protein Assay Kit (ThermoFisher). Meanwhile, protein G beads were washed five times and then diluted 1:1 with RIPA buffer and protease inhibitor. According to protein quantification calculations, 1 mg of protein extract (up to 800  $\mu$ l) was added to a new Eppendorf tube with 30  $\mu$ l of washed G beads to pre-clean samples. Tubes were kept on a rotator in a 4°C fridge to incubate for 1 h. Afterwards, using a magnetic rack, the supernatant was collected and transferred to a new Eppendorf tube with 2  $\mu$ g of FOXG1 antibody (Abcam; ab196868) and kept on a rotator overnight at 4°C.

On the second day, 30  $\mu$ l of washed G beads were added to the samples and incubated on the rotator at 4°C for at least 1 h. After, tubes were placed on the magnetic rack and the supernatant was discarded. Beads were washed six times with RIPA buffer and then resuspended in 150  $\mu$ l of Elution buffer. Beads were then incubated at 65°C for 10 min to elute the immunocomplexes from the beads. Tubes were then put on the magnetic rack—the supernatant was kept and beads were discarded. To the tube, 200 mM NaCl (6  $\mu$ l of 5 M NaCl) and 10  $\mu$ g of RNase A (10  $\mu$ l) were added for de-crosslinking. Samples were incubated overnight at 65°C.

On the third next day, 7.5  $\mu$ l of 10 mg/ml Proteinase K (Bio Basic) was added and tubes were incubated at 45°C for 2 h. Distilled water was added in a 1:1 ratio to dilute samples and then 600  $\mu$ l of DNA beads were added, mixed and incubated at room temperature for 5 min. Tubes were placed on the magnetic rack and the supernatant was removed. Samples were washed twice quickly with fresh 80% ethanol and aspirated. The bead pellet was dried on the magnetic rack for ~30 min. 50  $\mu$ l of ddH2O was added and incubated at 65°C in a bead bath for 5 min. Samples were then placed on the magnetic rack to separate beads and transfer the supernatant containing DNA to a final Eppendorf tube.

Final immunoprecipitated DNA fragments were 200–300 bp after initial sonication. DNA samples were sent to the Hospital for Sick Children where libraries were prepared using the NEB Ultra II DNA kit. Samples were sequenced on 1 lane Novaseq SP flowcell paired-end 2 × 100 bp.

## ChIP sequencing

The sequenced data was processed using the Nextflow chip-seq pipeline v 1.2.2 (80). First, raw sequencing reads (fastq files) were processed using the nf-core ChIPseq (version 1.2.1) processing template (80) for quality control (FastQC), adapter trimming (Trim Galore), and read alignment (BWA) against human genome version GRCh37/hg19 included with nf-core. Peak calling for FOXG1 binding was conducted using MACS2 (81) with the corresponding input as control. Preliminary analysis and annotation of peaks were done using Bioconductor R package ChIPseeker (v1.30.0) (82) mapped to hg19 (TxDb.Hsapiens.UCSC.hg19.knownGene\_3.2.2). Peaks containing FOXG1 DNA-binding motifs were assessed using bedtools getfasta function to extract sequences for the peak coordinates ( $\pm$  100 bp) contained in a bed file. Sequences were then parsed for any instances of the FOXG1 motif TRTTTRY (or reverse complement RYAAAAYA) where R = a purine (A/G) and Y = a pyrimidine (C/T). Peaks were filtered depending on whether a peak overlapped with a motif and the number of motifs were also calculated for each peak. Plots of ChIP peaks were generated with R packages karyoploteR (83) and custom script from bwtool (84).



## Transfection of FOXP1 into NPCs and western blot

Approximately  $1 \times 10^6$  NPCs were transfected with 3  $\mu\text{g}$  empty vector or FOXP1-Flag in a 6-cm dish using the Neon transfection system (Voltage: 1700 V, Width: 20 ms, Pulses: 1). Protein was extracted 48 h after transfection and assessed by western blot. Approximately 15  $\mu\text{g}$  of protein was loaded per well in Mini-PROTEAN TGX Stain-Free Precast Gels (Biorad). Gels were run at 150 V for approximately 75 min and then transferred to a nitrocellulose membrane using a Trans-Blot Turbo Transfer System (Biorad). Membranes were blocked in 4% non-fat milk dissolved in TBS-T buffer (tris-buffered saline-tritonX; Sigma-Aldrich) for 20 min and then incubated with primary antibodies overnight at 4°C with shaking. Blots were washed three times in TBS-T for 5 min and then incubated with appropriate mouse or rabbit secondary antibodies for 1 h at room temperature. Blots were washed another three times in TBST for 5 min, then imaged using a ChemiDoc XRS+ System (Biorad). Blots were imaged and analyzed using ImageLab (Biorad) software.

## FOXP1 over-expression in Case B cells

A wild-type CRISPR/CAS9-pRFP gene editing system was used to insert the FOXP1 over-expression (OE) construct (Supplementary Material, Fig. S9) into the safe harbor CLYBL locus. 1  $\mu\text{g}$  of construct was added per transfection reaction and transfection was carried out simultaneously with iPSC induction to ensure clonality, as previously described (34). After transfection, cells were selected for puromycin resistance and RFP visualization as described allowing for cell expansion from a single edited cell. Potentially edited colonies were expanded and stored as cell lines after which DNA was extracted and Sanger sequenced for insert integration.

## Statistical analysis

Data management and statistical analyses were done with R version 4.1.0. Error bars in ICC quantified plots represent the standard error of the mean (SEM). T-tests for significance were based on two-tailed student's t-tests. Statistical analyses and graphical outputs were generated using ggplot2. Statistical output and N are reported at all places data are reported. Visualization and analysis of ChIP peaks were done using the ChIPseeker package (82) and ChIP peak plots were generated using the karyoploteR package (83) in R.

## Supplementary Material

Supplementary Material is available at HMG online.

## Acknowledgements

We are grateful to the families of Case/Control A and Case/Control B for participating in this work.

*Conflict of interest statement.* The authors declare no conflicts of interest.

## Ethics statement

This work was approved by the Research Ethics Board of the Douglas Hospital Research Center, McGill University.

## Data availability

Request for materials should be made to the corresponding author, Carl Ernst.

## Funding

This work was supported by funding from the Fonds de Recherche de Québec—Santé (FRQS) doctoral program (N.C.H.); Indonesian Endowment Fund for Education PhD award (M.J.); The Crown Prince Court PhD Scholarship of the United Arab Emirates (S.A.); Consejo Nacional de Ciencia y Tecnología (CONACYT) program (Mexico) (L.A.); Canada Research Chairs program (C.E.); The FRQS Chercheurs Boursier-Senior program (C.E.) and the Canadian Institutes of Health Research (CIHR) scholarship (A.N. and A.S.) and CIHR Project grant (C.E.).

## Author contributions

C.E. and N.C.H. conceived the study and planned experiments. C.E. supervised all aspects of the project. N.C.H., H.P., P.F. and A.S. generated and cultured cell lines. N.C.H., A.S., P.S.S., M.-D.H. and J.-F.T. performed bioinformatic and statistical analyses of sequencing data. N.C.H., X.Z., A.N. and M.J. optimized chromatin immunoprecipitation protocols and N.C.H. performed ChIP experiments. H.P., Y.Z., L.A., X.Z. and S.A. grew and validated cell lines. N.C.H. and X.Z. validated FOXP1 antibodies for immunoprecipitation. X.Z., N.C.H. and H.P. performed western blots and genetic engineering experiments. N.C.H. and C.E. wrote the manuscript.

## References

- Ariani, F., Hayek, G., Rondinella, D., Artuso, R., Mencarelli, M.A., Spanhol-Rosseto, A., Pollazzon, M., Buoni, S., Spiga, O., Ricciardi, S. *et al.* (2008) FOXP1 is responsible for the congenital variant of Rett syndrome. *Am. J. Hum. Genet.*, **83**, 89–93.
- Philippe, C., Amsellem, D., Francannet, C., Lambert, L., Saunier, A., Verneau, F. and Jonveaux, P. (2010) Phenotypic variability in Rett syndrome associated with FOXP1 mutations in females. *J. Med. Genet.*, **47**, 59–65.
- Pringsheim, M., Mitter, D., Schroder, S., Warthemann, R., Plumacher, K., Kluger, G., Baethmann, M., Bast, T., Braun, S., Buttler, H.M. *et al.* (2019) Structural brain anomalies in patients with FOXP1 syndrome and in *Foxg1+/-* mice. *Ann. Clin. Transl. Neurol.*, **6**, 655–668.
- Murphy, D.B., Wiese, S., Burfeind, P., Schmundt, D., Mattei, M.G., Schulz-Schaeffer, W. and Thies, U. (1994) Human brain factor 1, a new member of the fork head gene family. *Genomics*, **21**, 551–557.
- Hettige, N.C. and Ernst, C. (2019) FOXP1 dose in brain development. *Front. Pediatr.*, **7**, 482.
- Hanashima, C., Li, S.C., Shen, L., Lai, E. and Fishell, G. (2004) *Foxg1* suppresses early cortical cell fate. *Science*, **303**, 56–59.
- Xuan, S., Baptista, C.A., Balas, G., Tao, W., Soares, V.C. and Lai, E. (1995) Winged helix transcription factor BF-1 is essential for the development of the cerebral hemispheres. *Neuron*, **14**, 1141–1152.
- Hanashima, C., Shen, L., Li, S.C. and Lai, E. (2002) Brain factor-1 controls the proliferation and differentiation of neocortical progenitor cells through independent mechanisms. *J. Neurosci.*, **22**, 6526–6536.
- Hettige, N.C., Peng, H., Wu, H., Zhang, X., Yerko, V., Zhang, Y., Jefri, M., Soubannier, V., Maussion, G., Alsuwaidi, S. *et al.* (2022) FOXP1 dose tunes cell proliferation dynamics in human forebrain progenitor cells. *Stem Cell Rep.*, **17**, 475–488.

10. Seoane, J., Le, H.V., Shen, L., Anderson, S.A. and Massague, J. (2004) Integration of Smad and forkhead pathways in the control of neuroepithelial and glioblastoma cell proliferation. *Cell*, **117**, 211–223.
11. Chen, J., Wu, X., Xing, Z., Ma, C., Xiong, W., Zhu, X. and He, X. (2018) FOXC1 expression is elevated in glioma and inhibits glioma cell apoptosis. *J. Cancer*, **9**, 778–783.
12. Verginelli, F., Perin, A., Dali, R., Fung, K.H., Lo, R., Longatti, P., Guiot, M.C., Del Maestro, R.F., Rossi, S., di Porzio, U. et al. (2013) Transcription factors FOXC1 and Groucho/TLE promote glioblastoma growth. *Nat. Commun.*, **4**, 2956.
13. Engstrom, P.G., Tommei, D., Stricker, S.H., Ender, C., Pollard, S.M. and Bertone, P. (2012) Digital transcriptome profiling of normal and glioblastoma-derived neural stem cells identifies genes associated with patient survival. *Genome Med.*, **4**, 76.
14. Cloughesy, T.F., Cavenee, W.K. and Mischel, P.S. (2014) Glioblastoma: from molecular pathology to targeted treatment. *Annu. Rev. Pathol.*, **9**, 1–25.
15. Siegenthaler, J.A., Tremper-Wells, B.A. and Miller, M.W. (2008) Foxg1 haploinsufficiency reduces the population of cortical intermediate progenitor cells: effect of increased p21 expression. *Cereb. Cortex*, **18**, 1865–1875.
16. Yip, D.J., Corcoran, C.P., Alvarez-Saavedra, M., DeMaria, A., Rennick, S., Mears, A.J., Rudnicki, M.A., Messier, C. and Picketts, D.J. (2012) Snf2l regulates Foxg1-dependent progenitor cell expansion in the developing brain. *Dev. Cell*, **22**, 871–878.
17. Furuta, Y., Piston, D.W. and Hogan, B.L. (1997) Bone morphogenetic proteins (BMPs) as regulators of dorsal forebrain development. *Development*, **124**, 2203–2212.
18. Manuel, M., Martynoga, B., Yu, T., West, J.D., Mason, J.O. and Price, D.J. (2010) The transcription factor Foxg1 regulates the competence of telencephalic cells to adopt subpallial fates in mice. *Development*, **137**, 487–497.
19. Vezzali, R., Weise, S.C., Hellbach, N., Machado, V., Heidrich, S. and Vogel, T. (2016) The FOXC1/FOXO/SMAD network balances proliferation and differentiation of cortical progenitors and activates Kcnn3 expression in mature neurons. *Oncotarget*, **7**, 37436–37455.
20. Dou, C., Lee, J., Liu, B., Liu, F., Massague, J., Xuan, S. and Lai, E. (2000) BF-1 interferes with transforming growth factor beta signaling by associating with Smad partners. *Mol. Cell Biol.*, **20**, 6201–6211.
21. Golson, M.L. and Kaestner, K.H. (2016) Fox transcription factors: from development to disease. *Development*, **143**, 4558–4570.
22. Tao, W. and Lai, E. (1992) Telencephalon-restricted expression of BF-1, a new member of the HNF-3/fork head gene family, in the developing rat brain. *Neuron*, **8**, 957–966.
23. Nakagawa, S., Gisselbrecht, S.S., Rogers, J.M., Hartl, D.L. and Bulyk, M.L. (2013) DNA-binding specificity changes in the evolution of forkhead transcription factors. *Proc. Natl. Acad. Sci. U. S. A.*, **110**, 12349–12354.
24. Dai, S., Li, J., Zhang, H., Chen, X., Guo, M., Chen, Z. and Chen, Y. (2020) Structural basis for DNA recognition by FOXC1 and the characterization of disease-causing FOXC1 mutations. *J. Mol. Biol.*, **432**, 6146–6156.
25. Kumamoto, T., Toma, K., Gunadi, M.K., McKenna, W.L., Kasukawa, T., Katzman, S., Chen, B. and Hanashima, C. (2013) Foxg1 coordinates the switch from nonradially to radially migrating glutamatergic subtypes in the neocortex through spatiotemporal repression. *Cell Rep.*, **3**, 931–945.
26. Cargnin, F., Kwon, J.S., Katzman, S., Chen, B., Lee, J.W. and Lee, S.K. (2018) FOXC1 orchestrates neocortical organization and cortico-cortical connections. *Neuron*, **100**, 1083–1096.e5.
27. Akol, I., Izzo, A., Gather, F., Strack, S., Heidrich, S., Ó hAilín, D., Villarreal, A., Hacker, C., Rauleac, T., Bella, C. et al. (2023) Multimodal epigenetic changes and altered NEUROD1 chromatin binding in the mouse hippocampus underlie FOXC1 syndrome. *Proc. Natl. Acad. Sci. U. S. A.*, **120**, e2122467120.
28. Dali, R., Verginelli, F., Pramatarova, A., Sladek, R. and Stifani, S. (2018) Characterization of a FOXC1:TLE1 transcriptional network in glioblastoma-initiating cells. *Mol. Oncol.*, **12**, 775–787.
29. Bell, S., Hettige, N.C., Silveira, H., Peng, H., Wu, H., Jefri, M., Antonyan, L., Zhang, Y., Zhang, X. and Ernst, C. (2019) Differentiation of human induced pluripotent stem cells (iPSCs) into an effective model of forebrain neural progenitor cells and mature neurons. *Bio Protoc.*, **9**, e3188.
30. Bell, S., Rousseau, J., Peng, H., Aouabed, Z., Priam, P., Theroux, J.F., Jefri, M., Tanti, A., Wu, H., Kolobova, I. et al. (2019) Mutations in ACTL6B cause neurodevelopmental deficits and epilepsy and lead to loss of dendrites in human neurons. *Am. J. Hum. Genet.*, **104**, 815–834.
31. McMahon, J.A., Takada, S., Zimmerman, L.B., Fan, C.M., Harland, R.M. and McMahon, A.P. (1998) Noggin-mediated antagonism of BMP signaling is required for growth and patterning of the neural tube and somite. *Genes Dev.*, **12**, 1438–1452.
32. Martynoga, B., Morrison, H., Price, D.J. and Mason, J.O. (2005) Foxg1 is required for specification of ventral telencephalon and region-specific regulation of dorsal telencephalic precursor proliferation and apoptosis. *Dev. Biol.*, **283**, 113–127.
33. Kim, J.H., Lee, S.R., Li, L.H., Park, H.J., Park, J.H., Lee, K.Y., Kim, M.K., Shin, B.A. and Choi, S.Y. (2011) High cleavage efficiency of a 2A peptide derived from porcine teschovirus-1 in human cell lines, zebrafish and mice. *PLoS One*, **6**, e18556.
34. Bell, S., Peng, H., Crapper, L., Kolobova, I., Maussion, G., Vasuta, C., Yerko, V., Wong, T.P. and Ernst, C. (2017) A rapid pipeline to model rare neurodevelopmental disorders with simultaneous CRISPR/Cas9 gene editing. *Stem Cells Transl. Med.*, **6**, 886–896.
35. Landt, S.G., Marinov, G.K., Kundaje, A., Kheradpour, P., Pauli, F., Batzoglou, S., Bernstein, B.E., Bickel, P., Brown, J.B., Cayting, P. et al. (2012) ChIP-seq guidelines and practices of the ENCODE and modENCODE consortia. *Genome Res.*, **22**, 1813–1831.
36. Lander, E.S., Linton, L.M., Birren, B., Nusbaum, C., Zody, M.C., Baldwin, J., Devon, K., Dewar, K., Doyle, M., FitzHugh, W. et al. (2001) Initial sequencing and analysis of the human genome. *Nature*, **409**, 860–921.
37. Kim, T.H., Barrera, L.O., Zheng, M., Qu, C., Singer, M.A., Richmond, T.A., Wu, Y., Green, R.D. and Ren, B. (2005) A high-resolution map of active promoters in the human genome. *Nature*, **436**, 876–880.
38. Heinz, S., Benner, C., Spann, N., Bertolino, E., Lin, Y.C., Laslo, P., Cheng, J.X., Murre, C., Singh, H. and Glass, C.K. (2010) Simple combinations of lineage-determining transcription factors prime cis-regulatory elements required for macrophage and B cell identities. *Mol. Cell*, **38**, 576–589.
39. Lorca, T. and Castro, A. (2013) The Greatwall kinase: a new pathway in the control of the cell cycle. *Oncogene*, **32**, 537–543.
40. Fatima, I., Singh, A.B. and Dhawan, P. (2020) MASTL: a novel therapeutic target for cancer malignancy. *Cancer Med.*, **9**, 6322–6329.
41. Meyerson, M. and Harlow, E. (1994) Identification of G1 kinase activity for cdk6, a novel cyclin D partner. *Mol. Cell Biol.*, **14**, 2077–2086.
42. Shen, T. and Huang, S. (2012) The role of Cdc25A in the regulation of cell proliferation and apoptosis. *Anti Cancer Agents Med. Chem.*, **12**, 631–639.

43. Ma, W., Stafford, L.J., Li, D., Luo, J., Li, X., Ning, G. and Liu, M. (2007) GCIP/CCNDBP1, a helix-loop-helix protein, suppresses tumorigenesis. *J. Cell. Biochem.*, **100**, 1376–1386.
44. Naeve, G.S., Ramakrishnan, M., Kramer, R., Hevroni, D., Citri, Y. and Theill, L.E. (1997) Neurtin: a gene induced by neural activity and neurotrophins that promotes neuritogenesis. *Proc. Natl. Acad. Sci. U. S. A.*, **94**, 2648–2653.
45. Vaags, A.K., Lionel, A.C., Sato, D., Goodenberger, M., Stein, Q.P., Curran, S., Ogilvie, C., Ahn, J.W., Drmic, I., Senman, L. et al. (2012) Rare deletions at the neurexin 3 locus in autism spectrum disorder. *Am. J. Hum. Genet.*, **90**, 133–141.
46. Fernandez, V., Llinares-Benadero, C. and Borrell, V. (2016) Cerebral cortex expansion and folding: what have we learned? *EMBO J.*, **35**, 1021–1044.
47. Yao, J., Lai, E. and Stifani, S. (2001) The winged-helix protein brain factor 1 interacts with groucho and hes proteins to repress transcription. *Mol. Cell. Biol.*, **21**, 1962–1972.
48. Chang, H.W., Li, J., Kretschmar, D. and Vogt, P.K. (1995) Avian cellular homolog of the qin oncogene. *Proc. Natl. Acad. Sci. U. S. A.*, **92**, 447–451.
49. Freyaldenhoven, B.S., Freyaldenhoven, M.P., Iacovoni, J.S. and Vogt, P.K. (1997) Avian winged helix proteins CWH-1, CWH-2 and CWH-3 repress transcription from Qin binding sites. *Oncogene*, **15**, 483–488.
50. Lam, E.W., Brosens, J.J., Gomes, A.R. and Koo, C.Y. (2013) Forkhead box proteins: tuning forks for transcriptional harmony. *Nat. Rev. Cancer*, **13**, 482–495.
51. Lalmansingh, A.S., Karmakar, S., Jin, Y. and Nagaich, A.K. (2012) Multiple modes of chromatin remodeling by Forkhead box proteins. *Biochim. Biophys. Acta*, **1819**, 707–715.
52. Tan, K., Shaw, A.L., Madsen, B., Jensen, K., Taylor-Papadimitriou, J. and Freemont, P.S. (2003) Human PLU-1 has transcriptional repression properties and interacts with the developmental transcription factors BF-1 and PAX9. *J. Biol. Chem.*, **278**, 20507–20513.
53. Marcal, N., Patel, H., Dong, Z., Belanger-Jasmin, S., Hoffman, B., Helgason, C.D., Dang, J. and Stifani, S. (2005) Antagonistic effects of Grg6 and Groucho/TLE on the transcription repression activity of brain factor 1/FoxG1 and cortical neuron differentiation. *Mol. Cell. Biol.*, **25**, 10916–10929.
54. Morillon, A., O'Sullivan, J., Azad, A., Proudfoot, N. and Mellor, J. (2003) Regulation of elongating RNA polymerase II by forkhead transcription factors in yeast. *Science*, **300**, 492–495.
55. Abbas, T. and Dutta, A. (2009) p21 in cancer: intricate networks and multiple activities. *Nat. Rev. Cancer*, **9**, 400–414.
56. Abastabar, M., Kheyrollah, M., Azizian, K., Bagherlou, N., Tehrani, S.S., Maniati, M. and Karimian, A. (2018) Multiple functions of p27 in cell cycle, apoptosis, epigenetic modification and transcriptional regulation for the control of cell growth: a double-edged sword protein. *DNA Repair (Amst)*, **69**, 63–72.
57. Creff, J. and Besson, A. (2020) Functional versatility of the CDK inhibitor p57(Kip2). *Front. Cell Dev. Biol.*, **8**, 584590.
58. Besson, A., Dowdy, S.F. and Roberts, J.M. (2008) CDK inhibitors: cell cycle regulators and beyond. *Dev. Cell*, **14**, 159–169.
59. Malumbres, M. (2014) Cyclin-dependent kinases. *Genome Biol.*, **15**, 122.
60. Zhang, P., Wong, C., DePinho, R.A., Harper, J.W. and Elledge, S.J. (1998) Cooperation between the Cdk inhibitors p27(KIP1) and p57(KIP2) in the control of tissue growth and development. *Genes Dev.*, **12**, 3162–3167.
61. Medema, R.H., Kops, G.J., Bos, J.L. and Burgering, B.M. (2000) AFX-like Forkhead transcription factors mediate cell-cycle regulation by Ras and PKB through p27kip1. *Nature*, **404**, 782–787.
62. Lizarraga, S.B., Margossian, S.P., Harris, M.H., Campagna, D.R., Han, A.P., Blevins, S., Mudbhary, R., Barker, J.E., Walsh, C.A. and Fleming, M.D. (2010) Cdk5rap2 regulates centrosome function and chromosome segregation in neuronal progenitors. *Development*, **137**, 1907–1917.
63. Nicholas, A.K., Swanson, E.A., Cox, J.J., Karbani, G., Malik, S., Springell, K., Hampshire, D., Ahmed, M., Bond, J., Di Benedetto, D. et al. (2009) The molecular landscape of ASPM mutations in primary microcephaly. *J. Med. Genet.*, **46**, 249–253.
64. Kumar, A., Girimaji, S.C., Duvvari, M.R. and Blanton, S.H. (2009) Mutations in STIL, encoding a pericentriolar and centrosomal protein, cause primary microcephaly. *Am. J. Hum. Genet.*, **84**, 286–290.
65. Guernsey, D.L., Jiang, H., Hussin, J., Arnold, M., Bouyakdan, K., Perry, S., Babineau-Sturk, T., Beis, J., Dumas, N., Evans, S.C. et al. (2010) Mutations in centrosomal protein CEP152 in primary microcephaly families linked to MCPH4. *Am. J. Hum. Genet.*, **87**, 40.
66. Gul, A., Hassan, M.J., Hussain, S., Raza, S.I., Chishti, M.S. and Ahmad, W. (2006) A novel deletion mutation in CENPJ gene in a Pakistani family with autosomal recessive primary microcephaly. *J. Hum. Genet.*, 760–764.
67. Fu, J., Hagan, I.M. and Glover, D.M. (2015) The centrosome and its duplication cycle. *Cold Spring Harb. Perspect. Biol.*, **7**, a015800.
68. Gonczy, P. (2012) Towards a molecular architecture of centriole assembly. *Nat. Rev. Mol. Cell Biol.*, **13**, 425–435.
69. Paul, L.K., Brown, W.S., Adolphs, R., Tyszka, J.M., Richards, L.J., Mukherjee, P. and Sherr, E.H. (2007) Agenesis of the corpus callosum: genetic, developmental and functional aspects of connectivity. *Nat. Rev. Neurosci.*, **8**, 287–299.
70. Edwards, T.J., Sherr, E.H., Barkovich, A.J. and Richards, L.J. (2014) Clinical, genetic and imaging findings identify new causes for corpus callosum development syndromes. *Brain*, **137**, 1579–1613.
71. Stoeckli, E. (2017) Where does axon guidance lead us? *F1000Res*, **6**, 78.
72. Schwarz, Q. and Ruhrberg, C. (2010) Neuropilin, you gotta let me know: should I stay or should I go? *Cell Adhes. Migr.*, **4**, 61–66.
73. Gonda, Y., Namba, T. and Hanashima, C. (2020) Beyond axon guidance: roles of slit-Robo signaling in neocortical formation. *Front. Cell Dev. Biol.*, **8**, 607415.
74. Tozer, S., Le Dreau, G., Marti, E. and Briscoe, J. (2013) Temporal control of BMP signalling determines neuronal subtype identity in the dorsal neural tube. *Development*, **140**, 1467–1474.
75. Bier, E. and De Robertis, E.M. (2015) EMBRYO DEVELOPMENT. BMP gradients: a paradigm for morphogen-mediated developmental patterning. *Science*, **348**, aaa5838.
76. Tuazon, F.B. and Mullins, M.C. (2015) Temporally coordinated signals progressively pattern the anteroposterior and dorsoventral body axes. *Semin. Cell Dev. Biol.*, **42**, 118–133.
77. Zinski, J., Tajer, B. and Mullins, M.C. (2018) TGF-beta family signaling in early vertebrate development. *Cold Spring Harb. Perspect. Biol.*, **10**, 1–75.
78. Langmead, B., Trapnell, C., Pop, M. and Salzberg, S.L. (2009) Ultrafast and memory-efficient alignment of short DNA sequences to the human genome. *Genome Biol.*, **10**, R25.
79. Trapnell, C., Roberts, A., Goff, L., Pertea, G., Kim, D., Kelley, D.R., Pimentel, H., Salzberg, S.L., Rinn, J.L. and Pachter, L. (2012) Differential gene and transcript expression analysis of RNA-seq experiments with TopHat and cufflinks. *Nat. Protoc.*, **7**, 562–578.
80. Ewels, P.A., Peltzer, A., Fillinger, S., Patel, H., Alneberg, J., Wilm, A., Garcia, M.U., Di Tommaso, P. and Nahnsen, S. (2020) The nf-core framework for community-curated bioinformatics pipelines. *Nat. Biotechnol.*, **38**, 276–278.



81. Feng, J., Liu, T., Qin, B., Zhang, Y. and Liu, X.S. (2012) Identifying ChIP-seq enrichment using MACS. *Nat. Protoc.*, **7**, 1728–1740.
82. Yu, G., Wang, L.G. and He, Q.Y. (2015) ChIPseeker: an R/Bioconductor package for ChIP peak annotation, comparison and visualization. *Bioinformatics*, **31**, 2382–2383.
83. Gel, B. and Serra, E. (2017) karyoploteR: an R/Bioconductor package to plot customizable genomes displaying arbitrary data. *Bioinformatics*, **33**, 3088–3090.
84. Pohl, A. and Beato, M. (2014) bwtool: a tool for bigWig files. *Bioinformatics*, **30**, 1618–1619.